

# MONITORING OF GAMMA-RAY BRIGHT AGN: THE MULTI-FREQUENCY POLARIZATION OF THE FLARING BLAZAR 3C 279<sup>†</sup>

SINCHEOL KANG<sup>1,2</sup>, SANG-SUNG LEE<sup>1,2</sup>, AND DO-YOUNG BYUN<sup>1</sup>

<sup>1</sup>Korea Astronomy and Space Science Institute, 776 Daedeok-daero, Yuseong, Daejeon 34055, Republic of Korea;  
kang87@kasi.re.kr, sslee@kasi.re.kr, bdy@kasi.re.kr

<sup>2</sup>University of Science and Technology, 217 Gajeong-ro, Yuseong-gu, Daejeon 34113, Republic of Korea

Received September xx, 2015; accepted October xx, 2015

**Abstract:** We present results of long-term multi-wavelength polarization observations of the powerful blazar 3C 279 after its  $\gamma$ -ray flare on 2013 December 20. We followed up this flare with single-dish polarization observations using two 21-m telescopes of the Korean VLBI Network. Observations carried out weekly from 2013 December 25 to 2015 January 11, at 22 GHz, 43 GHz, 86 GHz simultaneously, as part of the Monitoring Of GAMMA-ray Bright AGN (MOGABA) program. We measured 3C 279 total flux densities of 22–34 Jy at 22 GHz, 15–28 Jy (43 GHz), and 10–21 Jy (86 GHz), showing mild variability of  $\leq 50\%$  over the period of our observations. The spectral index between 22 GHz and 86 GHz ranged from  $-0.13$  to  $-0.36$ . Linear polarization angles were  $27^\circ$ – $38^\circ$ ,  $30^\circ$ – $42^\circ$ , and  $33^\circ$ – $50^\circ$  at 22 GHz, 43 GHz, and 86 GHz, respectively. The degree of linear polarization was in the range of 6–12%, and slightly decreased with time at all frequencies. We investigated Faraday rotation and depolarization of the polarized emission at 22–86 GHz, and found Faraday rotation measures (RM) of  $-300$  to  $-1200$  rad  $m^{-2}$  between 22 GHz and 43 GHz, and  $-800$  to  $-5100$  rad  $m^{-2}$  between 43 GHz and 86 GHz. The RM values follow a power law with a mean power law index  $a$  of 2.2, implying that the polarized emission at these frequencies travels through a Faraday screen in or near the jet. We conclude that the regions emitting polarized radio emission may be different from the region responsible for the 2013 December  $\gamma$ -ray flare and are maintained by the dominant magnetic field perpendicular to the direction of the radio jet at milliarcsecond scales.

**Key words:** galaxies: active — galaxies: jets — galaxies: magnetic fields — polarization — quasars: individual (3C 279)

## 1. INTRODUCTION

Active Galactic Nuclei (AGN) are among the most spectacular objects in the Universe. They produce enormous luminosities ( $\sim 10^{42}$  to  $\sim 10^{48}$  erg  $s^{-1}$ ) in compact regions (i.e.,  $\ll 1pc^3$ ) and radiate broadband continuum emission from radio to  $\gamma$ -ray (up to TeV energies) with often highly variable and polarized emission detected in particular at radio, optical, and  $\gamma$ -ray (see, e.g., Krolik 1999). AGN are known to be powered by accretion of gas onto supermassive black holes (SMBH,  $M_{BH} \approx 10^6 - 10^9 M_\odot$ ), launching relativistic outflows (jets) perpendicular to the accretion disk plane into interstellar space (see e.g., Boettcher et al. 2012, for a review). AGN with relativistic jets roughly aligned with our line of sight (e.g., viewed within  $\sim 20^\circ$  from the jet axis) are commonly called blazars. Characteristic properties of blazars are strong continuum emission, rapid variability, high polarization (at radio and optical), and sometimes a lack of significant emission lines. The high apparent Lorentz factors in the relativistic jets lead to amplification (boosting) of the continuum emission by the fourth power of the relativistic

Doppler factor (Krawczynski et al. 2012). The narrow viewing angles and relativistic flows often lead to dramatic variations in total flux and polarization over the full spectrum.

Within last 7 years,  $\gamma$ -ray bursts (or flares) have been reported from more than 100 AGN, including 3C 273<sup>1</sup>, 4C +21.35<sup>2</sup>, 3C 454.3<sup>3</sup>, and 1510-089<sup>4</sup>, by the Large Area Telescope on the Fermi Gamma-ray Space Telescope<sup>5</sup>. Subsequent studies of the correlation between emission at  $\gamma$ -ray and other wavelengths have been aimed at revealing, e.g., the origin and location of the  $\gamma$ -ray flares in AGN, the dominating emission mechanisms of the high energy radiation (including  $\gamma$ -rays), and the role of magnetic fields in  $\gamma$ -ray flares. For example, Marscher et al. (2010) compare the  $\gamma$ -ray light curve of PKS 1510-089 against other wavelengths using data obtained while the source flared at  $\gamma$ -ray during 2009.0~2009.5. They find that the  $\gamma$ -ray peak coincides with the optical peak. They further find that the optical electric vector position angle (EVPA) rotated more

<sup>1</sup>Atel #2200: [www.astronomerstelegam.org/?read=2200](http://www.astronomerstelegam.org/?read=2200)

<sup>2</sup>Atel #2584: [www.astronomerstelegam.org/?read=2584](http://www.astronomerstelegam.org/?read=2584)

<sup>3</sup>Atel #3041: [www.astronomerstelegam.org/?read=3041](http://www.astronomerstelegam.org/?read=3041)

<sup>4</sup>Atel #3473: [www.astronomerstelegam.org/?read=3473](http://www.astronomerstelegam.org/?read=3473)

<sup>5</sup><http://fermi.gsfc.nasa.gov>

CORRESPONDING AUTHOR: Sang-Sung Lee

<sup>†</sup>Part of a special issue on the Korean VLBI Network (KVN)



**Table 1**  
Summary of our observations

Dates		$\nu$ (GHz) : HPBW (arcsec) : $\eta$		
MJD	Calendar	TN	US	YS
56651-56991 <sup>a</sup>	2013.12.25 – 2014.11.30	22.400 : 125 : 0.58 43.100 : 61 : 0.60	—	43.122 : 63 : 0.64 86.243 : 32 : 0.49
56992-57022 <sup>b</sup>	2014.12.01 – 2014.12.31	—	22.400 : 124 : 0.61 43.100 : 63 : 0.62	43.122 : 63 : 0.64 86.243 : 32 : 0.49
57022-57033 <sup>b</sup>	2015.01.01 – 2015.01.11	—	22.400 : 124 : 0.63 43.100 : 63 : 0.61	43.122 : 63 : 0.63 86.243 : 32 : 0.50

a: epoch 1; b: epoch 2; in epoch 1, we did not conduct observations from 2013.6.14 to 2013.8.22 due to KVN summer maintenance.

Before each observing session, we corrected antenna pointing offsets and measured the total flux density (i.e., Stokes I) using cross-scan observations of the source. All observations followed antenna gain calibration measurements. To track changes in atmospheric opacity, once between every two polarization observations we measured the system temperature at eight elevations, 18.21°, 20.17°, 22.62°, 25.77°, 30.00°, 36.03°, 45.58°, and 65.38° (so-called sky tipping curve measurements). The typical optical depths during our observations were 0.06–0.08, 0.16–0.18, and 0.12–0.15 in the 22 GHz, 43 GHz, and 86 GHz bands, respectively.

To calibrate the polarization angle, the Crab nebula was observed in each session (i.e., about once per seven days). The polarization angle of the Crab nebula at the KVN operating frequencies is well known and stable in time (Flett & Henderson 1979; Aumont et al. 2010). Planets, such as Venus, Jupiter, or Mars were observed in each session for calibrating the instrumental polarization, based on the assumption that their emission is unpolarized. To ensure the reliability of the polarization calibration, the standard polarization calibrator 3C 286 was observed once per session as well. We calibrated the absolute flux density scale with antenna gain measurements using planets and the antenna gain–elevation curve (Lee et al. 2011). All observations were made at elevations between 30° and 70°, since according to the KVN status report of 2014, the antenna gains are stable in this elevation range<sup>8</sup>.

## 2.2. Data Reduction

We processed the polarimetric observations using the data processing software developed by Byun et al. (in prep.), which we briefly describe in this section. The KVN digital spectrometer backend used for single-dish polarimetric observations outputs two single-polarization spectra ( $v_{ll^*}$  and  $v_{rr^*}$ ), and one complex cross-polarization spectrum ( $v_{lr^*}$  or  $v_{rl^*}$ , where  $v_{rl^*}$  is the complex conjugate of  $v_{lr^*}$ ) separated into real and imaginary parts ( $R_{rl^*}$  and  $I_{rl^*}$ ). All four Stokes parameters,  $I$ ,  $Q$ ,  $U$ , and  $V$ , can be estimated from these four polarization outputs using the following equations (Sault et al. 1996):

$$v_{ll^*} = \frac{1}{2} g_l g_l^* (I + V) \quad (1)$$

$$v_{lr^*} = \frac{1}{2} g_l g_r^* [(d_l - d_r^*) I + e^{-2i\chi_{\text{PA}}} (Q + iU)] \quad (2)$$

$$v_{rl^*} = \frac{1}{2} g_r g_l^* [(d_l^* - d_r) I + e^{2i\chi_{\text{PA}}} (Q - iU)] \quad (3)$$

$$v_{rr^*} = \frac{1}{2} g_r g_r^* (I - V) \quad (4)$$

where  $v_{ll^*}$ ,  $v_{lr^*}$ ,  $v_{rl^*}$  and  $v_{rr^*}$  are spectrometer outputs of circular feed horns, the subscripts  $l$ ,  $r$ ,  $l^*$ , and  $r^*$  indicate left-handed and right-handed circular polarizations and their complex conjugates, respectively,  $g_l$  and  $g_r$  are complex gain factors,  $d_l$  and  $d_r$  are complex terms describing cross-polarization leakage ( $d_l$ : LCP to RCP,  $d_r$ : RCP to LCP), i.e., the D-term, and  $\chi_{\text{PA}}$  is the parallactic angle. With the polarization outputs from the KVN spectrometer, we were able to determine the complex spectra of so-called combined-D-term  $d_l - d_r^*$  (or  $d_r - d_l^*$ ) by observing unpolarized sources such as Jupiter, Venus, or Mars, as shown in Figure 1a for the amplitude and in Figure 1b for the phase, assuming the Stokes parameters  $V = Q = U = 0$  for the unpolarized sources. Then, we estimated the four Stokes parameters, i.e.,  $I$ ,  $Q$ ,  $U$ , and  $V$  for the target sources.

From the estimated Stokes parameters, we obtained the total flux density,  $I$ , the degree of linear polarization,  $p = \sqrt{Q^2 + U^2}/I$ , and the polarization angle  $\chi = (1/2) \times \arctan(U/Q)$ , as shown in Figure 2. The estimated polarization angle is converted to the intrinsic polarization angle by comparing the estimated polarization angle against the known angle of a primary angle calibrator, like the Crab nebula. We used  $\chi = 154^\circ \pm 2^\circ$  for the Crab nebula at 22–86 GHz bands (Flett & Henderson 1979; Aumont et al. 2010). We evaluated the polarization observations by calibrating the linear polarization angles of 3C 286 when available. This target has stable polarization angles of  $35 \pm 0.2^\circ$  at 23 GHz, and  $35.8 \pm 0.1^\circ$  at 45 GHz (Perley & Butler 2013). The polarization angles of 3C 286 obtained from our KVN observations at 22 GHz and 43 GHz are shown in Figure 3. They are largely consistent with those of Perley & Butler.

We flagged 3C 279 polarization measurements in a session when the polarization angle of 3C 286 at 22 GHz or 43 GHz deviated from its intrinsic value or when the polarization angle uncertainty of 3C 279 was larger than the expected value. The rms uncertainties of the linear polarization observations due to the thermal noise were

<sup>8</sup>[http://kvn.kasi.re.kr/status\\_report\\_2014](http://kvn.kasi.re.kr/status_report_2014)

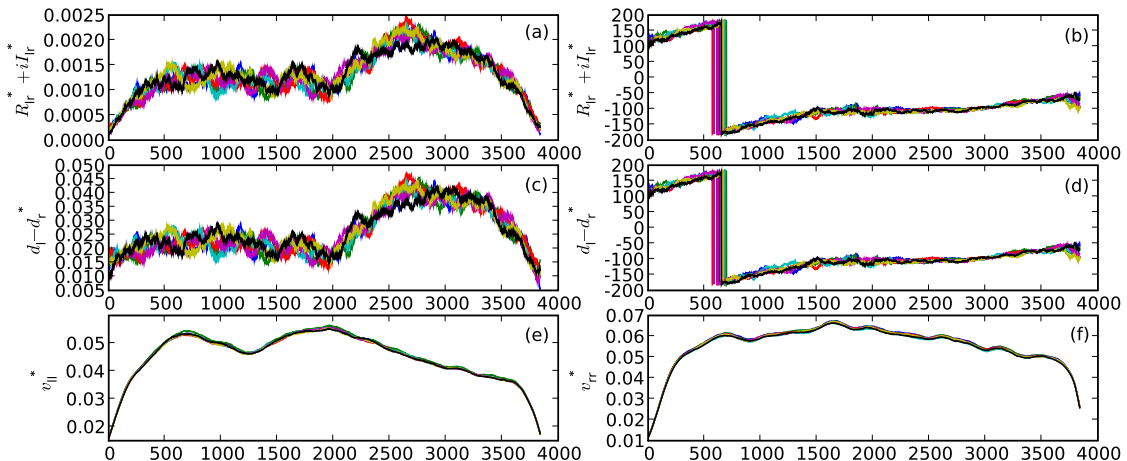


**Figure 1.** Spectrometer outputs for Jupiter. (a) and (b) are the amplitude and phase of  $R_{r1}^* + iI_{r1}^*$ , respectively, (c) and (d) are the amplitude and phase of  $d_l - d_r^*$ , respectively. (e) is  $v_{ll}^*$ , and (f) is  $v_{rr}^*$ . Colors indicate the 8 sets of measurements.

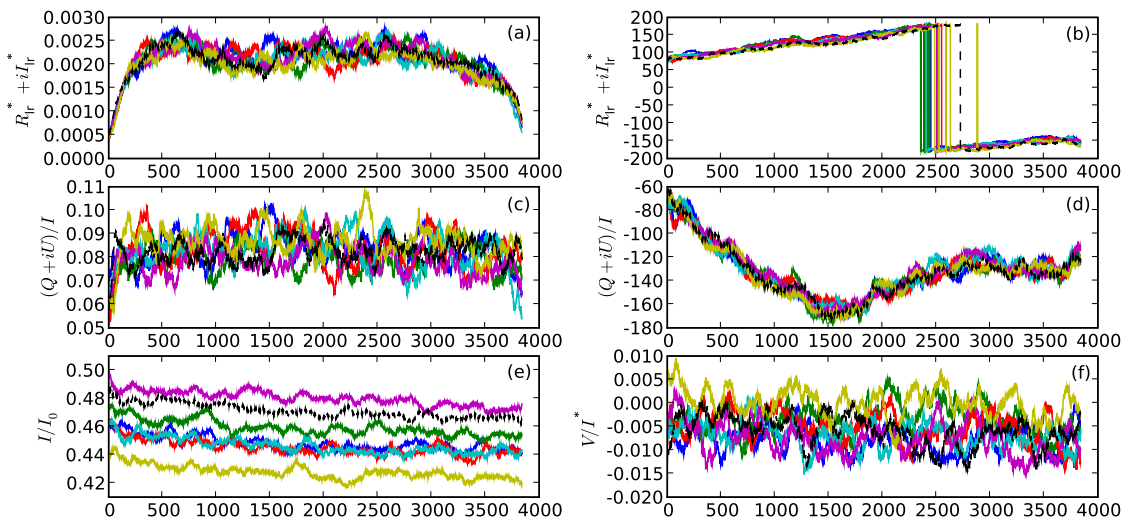


**Figure 2.** Spectrometer outputs for 3C 279. (a) and (b) are the amplitude and phase of  $R_{r1}^* + iI_{r1}^*$ , (c) and (d) are the amplitude and phase of  $\frac{Q+iU}{I}$ , respectively. (e) is  $\frac{I}{I_0}$ , and (f) is  $\frac{V}{I}$ . Colors indicate the 8 sets of measurements.

about 10 mJy and 15 mJy at 22 GHz and 43 GHz, respectively. The systematic error of the polarization angle measurements was  $\sim 2^\circ$  at both frequencies due to the uncertainty of the polarization angle of the Crab nebula. The typical instrumental polarization leakage of the KVN system is  $< 5\%$  at both frequencies, e.g., as shown in Figure 1c.

We also obtained the total flux density of 3C 279 from the cross scan observations taking into account the antenna pointing corrections as

$$T_{A,az}^* = T_{A,az,o}^* \times \exp\left(4 \ln 2 \frac{EL_{\text{off}}}{HPBW}\right)$$

and

$$T_{A,el}^* = T_{A,el,o}^* \times \exp\left(4 \ln 2 \frac{AZ_{\text{off}}}{HPBW}\right),$$

where  $T_{A,az,o}^*$  and  $T_{A,el,o}^*$  are the peak values of the observed antenna temperatures for azimuth and elevation

scans, respectively,  $HPBW$  is half power beam width of a KVN single-dish antenna, and  $EL_{\text{off}}$  and  $AZ_{\text{off}}$  are the pointing offsets in the azimuth and elevation directions, respectively. We obtained the averaged peak value  $T_A$  and converted it to the source flux density as  $S_\nu = 2kT/(\eta A_g)$ , where  $k$  is the Boltzmann constant, and  $\eta$  and  $A_g$  are the aperture efficiency and area of a KVN single-dish antenna. For each observing epoch we adopted appropriate values for  $HPBW$  and  $A_g$  (see Table 1) from the annual KVN status reports.

### 3. RESULTS

Our multi-frequency simultaneous polarization monitoring observations between 2013 December 25 and 2015 January 11 obtained 3C 279 total flux densities  $S_\nu$  of 22–34 Jy, 15–28 Jy, and 10–21 Jy at 22 GHz, 43 GHz, and 86 GHz, respectively. The respective light curves are shown in Figure 4 (top) and are summarized in Table 2.

**Table 2**  
Results of multi-frequency polarization observations for 3C 279. Uncertainties are  $1\sigma$ .

MJD	22 GHz			43 GHz			86 GHz		
	$S_\nu$ (Jy)	$\chi$ ( $^\circ$ )	$p$ (%)	$S_\nu$ (Jy)	$\chi$ ( $^\circ$ )	$p$ (%)	$S_\nu$ (Jy)	$\chi$ ( $^\circ$ )	$p$ (%)
56649.86	29.4±0.01	34.8±0.07	9.2±0.02	25.7±0.01	31.6±0.11	10.0±0.01	18.6±0.02	36.4±0.21	9.6±0.05
56654.82				26.1±0.01	36.3±0.14	9.5±0.01	20.4±0.02	42.6±0.17	9.4±0.06
56655.84				24.6±0.01	36.8±0.06	9.8±0.01	16.4±0.02	41.6±0.64	10.4±0.05
56656.81	29.5±0.01	32.4±0.05	9.6±0.02	26.2±0.01	37.9±0.35	9.7±0.02	20.5±0.02	41.1±0.21	10.2±0.03
56657.83	30.3±0.01	33.7±0.04	9.5±0.02	25.7±0.01	36.2±0.08	9.7±0.02	14.8±0.02	41.8±0.29	10.0±0.05
56670.77	30.9±0.01	30.3±0.01	9.8±0.01	26.3±0.01	35.6±0.17	10.0±0.02	17.3±0.02	39.4±0.18	10.7±0.05
56674.77				26.2±0.01	32.3±0.17	10.1±0.01	19.3±0.02	34.9±0.15	10.6±0.04
56682.78	30.9±0.01	29.5±0.24	9.6±0.02	26.5±0.01	31.7±0.07	9.5±0.01	18.6±0.01	36.4±0.15	9.7±0.04
56693.76				27.8±0.01	30.9±0.06	9.6±0.01	20.5±0.02	33.8±0.15	10.1±0.03
56700.77				27.8±0.01	31.8±0.08	9.8±0.02	20.1±0.02	35.1±0.11	10.5±0.03
56703.72				27.9±0.01	30.5±0.10	9.8±0.01	17.7±0.02	35.8±0.34	10.4±0.06
56714.65	33.0±0.01	29.9±0.04	9.4±0.02	28.0±0.01	34.4±0.15	10.0±0.01	19.9±0.02	39.5±0.22	11.0±0.03
56722.66	31.7±0.01	32.1±0.02	9.9±0.01	27.0±0.01	34.7±0.05	10.5±0.01	19.4±0.02	40.0±0.07	11.8±0.03
56742.63	32.2±0.01	28.2±0.01	9.9±0.02						
56757.55	29.2±0.01	34.4±0.06	9.3±0.02	24.9±0.01	36.8±0.06	9.9±0.01	16.2±0.02	43.9±0.19	10.5±0.08
56765.51	29.3±0.02	33.6±0.10	9.0±0.02						
56768.52	29.2±0.02	31.9±0.08	8.9±0.02	24.2±0.01	37.4±0.09	9.8±0.01	18.2±0.02	44.4±0.20	11.0±0.06
56782.47	28.6±0.01	32.4±0.54	8.9±0.04						
56790.44	28.4±0.01	35.1±0.08	8.6±0.01	23.5±0.01	37.7±0.11	9.3±0.03	15.1±0.02	44.3±0.27	10.3±0.13
56798.43	28.9±0.01	37.6±0.57	8.5±0.04						
56814.45				22.6±0.01	41.1±0.34	9.0±0.02	16.1±0.03	41.1±0.59	9.4±0.09
56897.20	33.1±0.09	31.8±0.11	6.8±0.20	19.2±0.01	38.6±0.22	7.6±0.05	12.0±0.03	45.0±0.56	7.7±0.35
56900.17	29.6±0.08	30.5±0.53	6.4±0.08	20.3±0.01	36.8±0.19	7.5±0.05	15.2±0.03	43.1±1.10	8.6±0.33
56905.19	27.4±0.05	34.2±0.17	6.3±0.10	17.2±0.05	42.0±0.16	8.3±0.16			
56911.13	29.7±0.05	27.9±0.20	6.5±0.05						
56915.17	27.3±0.08	28.2±0.18	6.0±0.06						
56920.13				20.9±0.01	33.5±0.36	6.4±0.05	16.6±0.02	43.8±1.31	8.1±0.16
56994.90	24.6±0.01	32.0±0.16	7.7±0.07	15.4±0.01	38.5±0.06	8.4±0.03	10.2±0.01	49.2±0.49	9.2±0.09
56999.90				18.6±0.01	38.8±0.12	7.9±0.02	11.8±0.01	48.0±0.24	8.7±0.05
57007.88	22.8±0.01	35.2±0.57	7.2±0.05	18.9±0.01	40.0±0.06	7.9±0.01	12.5±0.01	46.6±0.09	9.1±0.07
57014.80	23.8±0.01	30.8±0.09	6.7±0.02						
57019.83	23.6±0.01	32.8±0.14	6.6±0.01						
57026.82				18.9±0.01	42.1±0.23	7.1±0.02	14.2±0.02	43.8±0.21	9.2±0.05
57033.78	23.0±0.01	32.3±0.28	7.2±0.02	18.7±0.01	40.4±0.21	7.5±0.02	13.3±0.02	46.8±0.18	8.8±0.08
57040.78	24.0±0.01	31.0±0.45	8.4±0.09						

The flux densities exhibit a mild global decrease with time of  $<50\%$ , with no prominent flares over a period of about 390 days (MJD 56650–57040), and were almost constant or slightly increasing over a period of about 80 days (MJD 56650–57040).

The spectral index,  $\alpha$  ( $S_\nu \propto \nu^\alpha$ ), between the 22 GHz and 86 GHz bands ranges from  $-0.13$  to  $-0.36$ , implying that 3C 279 is a flat spectrum source. Its spectral index showed mild variability for about a year after the 2013 December giant  $\gamma$ -ray flare.

The linear polarization angle  $\chi$  of 3C 279 is shown in Figure 4 (middle), and is in the range of  $27^\circ$ – $38^\circ$ ,  $30^\circ$ – $42^\circ$ , and  $33^\circ$ – $50^\circ$  at 22 GHz, 43 GHz, and 86 GHz, respectively. After the giant  $\gamma$ -ray flare, the polarization angle rotated by  $\sim 10^\circ$  on a timescale of  $\sim 50$  days.

Faraday rotation scales with the square of the observing wavelength,  $\lambda$ , like  $\chi_{\text{obs}} = \chi_{\text{int}} + \text{RM}\lambda^2$ . Using the polarization angles observed at 22–86 GHz, we estimate the rotation measure, RM, of the Faraday rotation of the polarized radio emission from 3C 279. The resulting RMs are shown in Figure 5 (middle). We find rotation

measures in the range from  $-300$  to  $-1200$   $\text{rad m}^{-2}$  between the 22 GHz and 43 GHz bands, and from  $-800$  to  $-5100$   $\text{rad m}^{-2}$  between the 43 GHz and 86 GHz bands, respectively. An exception was the first measurement on MJD 56650 with a positive RM of about  $+500$   $\text{rad m}^{-2}$  between the 22 GHz and 43 GHz bands, leading to a RM change of about  $-1300$   $\text{rad m}^{-2}$  until the next measurement on MJD 56657.

The degree of linear polarization,  $p$ , of 3C 279 measured in the 22–86 GHz bands is in the range of  $6\%$ – $12\%$ . It exhibits a slightly decreasing trend with time over the whole period of observations. About 70 days after the giant  $\gamma$ -ray flare, the degree of linear polarization at 86 GHz showed a short-term increase from  $\sim 10\%$  to  $\sim 12\%$ , whereas the polarization fraction at other frequencies remained almost constant. After MJD 56750 the degree of linear polarization at all frequency bands started to decrease with time, and remained at low levels of around  $6\%$ – $9\%$ , although there are observation gaps due to KVN maintenance.

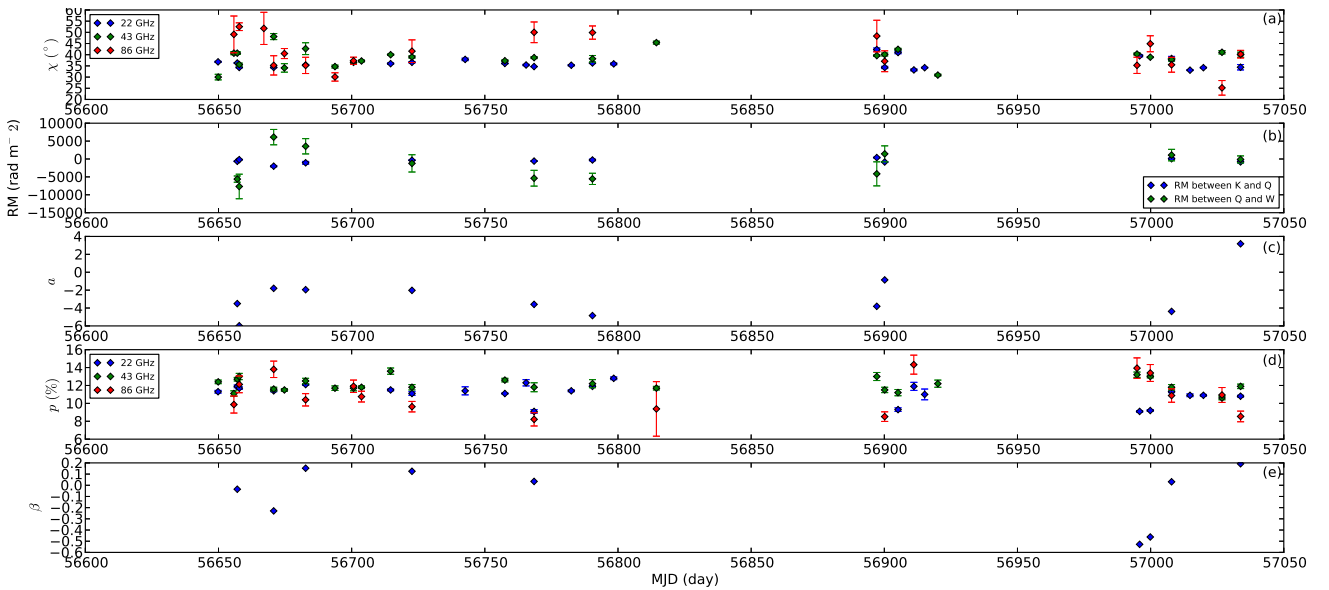


**Figure 3.** Light curves of a comparison source 3C 286 for (a) the linear polarization angle ( $^{\circ}$ ), (b) the Faraday rotation measure RM ( $\text{rad m}^{-2}$ ), (c) the  $a$  index, (d) the degree of linear polarization (%), and (e) the depolarization index  $\beta$ , at 22 GHz (red), 43 GHz (green), and 86 GHz (blue) from 2013 December to 2015 March. 3C 286 is much fainter at 86 GHz than at 22 and 43 GHz, so the uncertainty of the polarization observations due to thermal noise is larger. The  $a$  index and the depolarization index  $\beta$  are derived when the polarization measurements at three frequency bands are available.

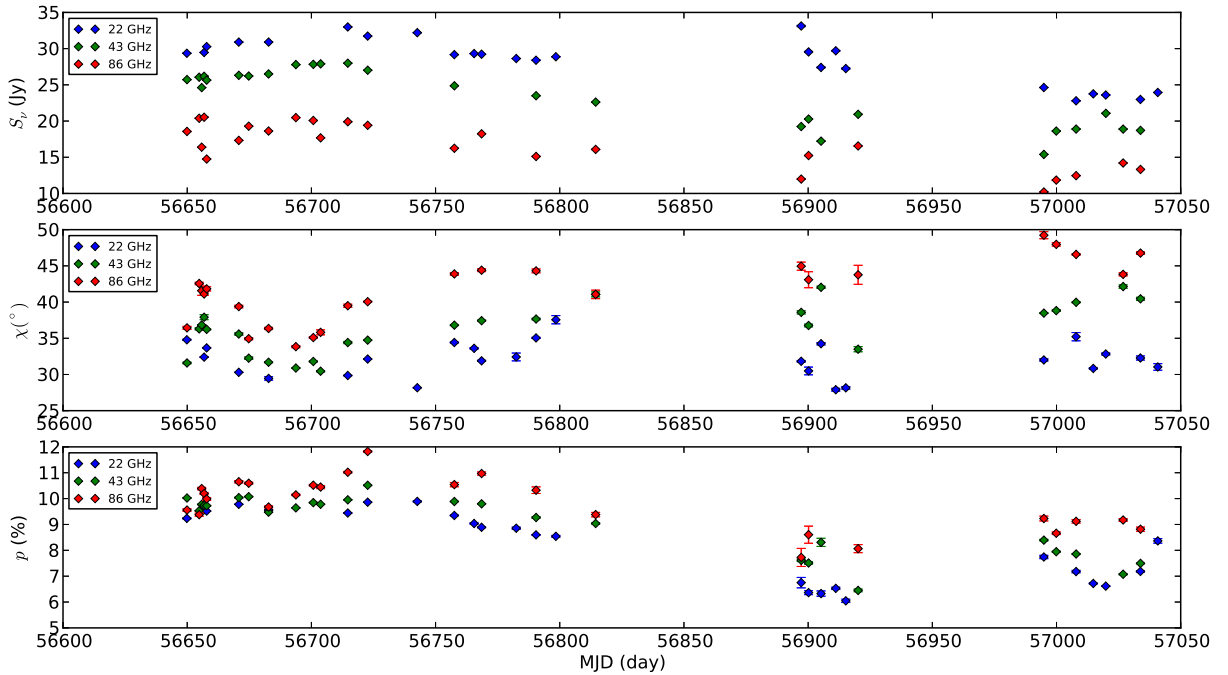


**Figure 4.** Light curves of 3C 279 for the total flux density (top) measured with the cross-scan observations, the linear polarization angle ( $^{\circ}$ ) (middle), and the degree of linear polarization (%) (bottom), at 22 GHz (red), 43 GHz (green), and 86 GHz (blue) from 2013 December to 2015 March.

#### 4. DISCUSSION AND CONCLUSIONS

The multi-frequency light curves in total flux density of 3C 279 at the 22 GHz, 43 GHz, and 86 GHz bands show a mild global decrease with time of  $<50\%$  with no prominent flares over a period of  $\sim 390$  days (MJD 56650–57040), and are almost constant or slightly in-

creasing over a period of  $\sim 80$  days (MJD 56650–56730), maintaining the characteristics of a flat-spectrum radio quasar with a spectral index of  $\alpha = -0.13 \sim -0.36$ . We do not find a flaring brightening by a factor of  $> 5$ , which would be expected for a radio counterpart to the strong  $\gamma$ -ray flare detected in 2013 December (MJD 56650) (see Figure 1 in Hayashida et al. 2015). The

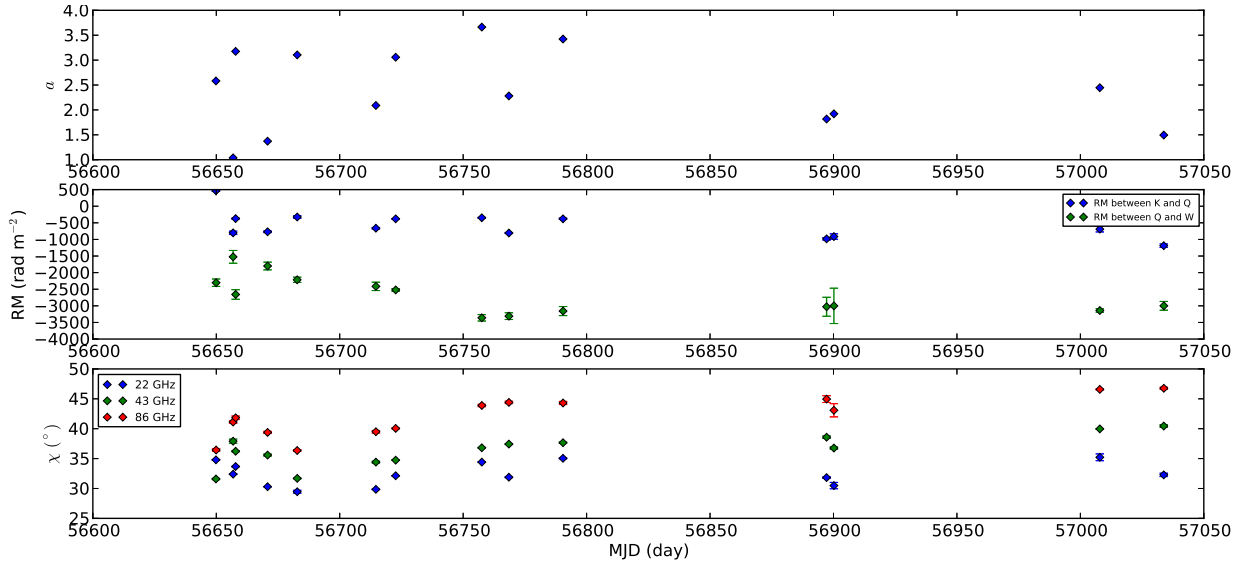


**Figure 5.** Plots of index  $a$  (top), the Faraday rotation measure  $RM$  ( $\text{rad m}^{-2}$ ) (middle), and the linear polarization angle ( $^\circ$ ) (bottom) of 3C 279 at 22 GHz (red), 43 GHz (green), and 86 GHz (blue). Measurements are shown only when the measurements at three frequency bands are available for estimating the index  $a$  in the relation  $|RM(\nu)| \propto \nu^a$ .

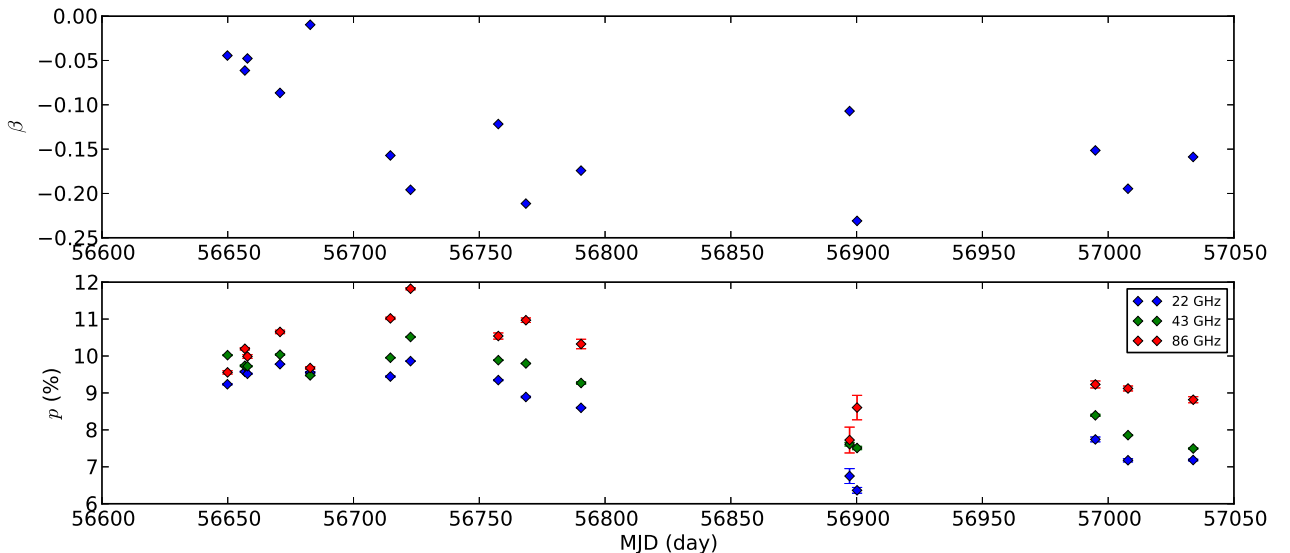


**Figure 6.** Plots of depolarization index  $\beta$  (top) and the degree of linear polarization (bottom) of 3C 279 at 22 GHz (red), 43 GHz (green), and 86 GHz (blue). Measurements are shown only when the measurements at three frequency bands are available for estimating  $\beta$  index. The green solid line is the best fit result of the linear model to the data.

lack of such a radio flare may imply that the radio and  $\gamma$ -ray emission are generated by different populations of electrons, and at different locations, as indicated by Hayashida et al. (2015) for the X-ray, optical, and millimeter (230 GHz) bands. A similar report on the poor correlation of the light curves at radio (5, 15, 37, and 230 GHz) and  $\gamma$ -ray after the giant  $\gamma$ -ray flares in 2009 was given by Abdo et al. (2010), indicating that the emission region responsible for the  $\gamma$ -ray flares is optically thick at radio wavelengths. It is possible that we have missed radio counterparts to the  $\gamma$ -ray flare, if these occurred right after the  $\gamma$ -ray peak on 2013 December 20, as there was a 4-day delay between the  $\gamma$ -ray flare and the start of our observations. However,

this possibility can be excluded by the 230 GHz light curve obtained before and after the gamma-ray peak as reported by Hayashida et al. (2015), where no prominent flare is detected, assuming that any gamma-ray flare optically thin at 22–86 GHz should be most likely optically thin at 230 GHz as well. Therefore, we suggest that the 2013 December  $\gamma$ -ray flare of 3C 279 originated in an emission region that is optically thick at radio frequencies of 22–86 GHz, or may be generated by different populations of electrons at locations different from those for the radio emission.

The linear polarization angle at 22–86 GHz bands showed no fast rotation over the time period of observations, and remained between  $22^\circ$  and  $50^\circ$  with a

median angle of  $\sim 36^\circ$ . The intrinsic polarization angles corrected for Faraday rotation ranged from  $30^\circ$  to  $53^\circ$  with a median angle of  $\sim 42^\circ$ , which is aligned to the jet direction of  $\sim -142^\circ$  observed by the KVN at 22–129 GHz (Lee et al. 2015). The radio polarization angle shows a behavior similar to the optical polarization angle over MJD 56615 and 56775 as reported by Hayashida et al. (2015) who reported an optical polarization angle around  $50^\circ$ . The degree of linear polarization shows no prominent change or correlation corresponding to the  $\gamma$ -ray flare, although there were local enhancements or a global decrease with time of  $<50\%$ . These imply that the radio and optical polarization emission regions may be different from the region responsible for the  $\gamma$ -ray flare and are maintained by the dominant magnetic field perpendicular to the direction of the radio jet at milliarcseconds scales.

For further investigation of the multi-frequency radio polarization of 3C 279, the degree of linear polarization at 22–86 GHz bands was fitted with a power law function of  $p(\%) = A\lambda^\beta$ , suggested by Tribble (1991) and Farnes et al. (2014), where  $A$  is constant,  $\beta$  is a polarization spectral index, and  $\lambda$  is the observing wavelength in cm. The best fit results of the power law model to the data are shown in Figure 6, yielding  $\beta = -0.01 \sim -0.23$ . Since the power law model of the degree of linear polarization explains the effect of external Faraday depolarization at longer wavelengths (see Burn 1966), the best fit results indicate that the effect of external Faraday depolarization is very small within the polarization regions corresponding to the observing beams ( $30'' - 130''$ ) of the KVN single-dish radio telescopes. This result seems in contradiction to the relatively high values of the estimated Faraday rotation RM from  $-300$  to  $-1200 \text{ rad m}^{-2}$  between the 22 GHz and 43 GHz bands, and from  $-800$  to  $-5100 \text{ rad m}^{-2}$  between the 43 GHz and 86 GHz bands. However, as suggested by Lee et al. (2015) for the multi-frequency polarization at a single epoch within the period of our observations, these results indicate that the polarization emission of 3C 279 at 22–86 GHz bands travels through a Faraday screen containing a uniform magnetic field that either persisted for  $\sim 400$  days after the  $\gamma$ -ray flare, or was not affected by the  $\gamma$ -ray events.

The stable, global characteristic of the magnetic field in the Faraday screen, unaffected by the  $\gamma$ -ray flare, suggest that the Faraday screen may be located away from the regions corresponding to the  $\gamma$ -ray flare so that the distribution of the dominant magnetic field is decoupled from the  $\gamma$ -ray flaring mechanism. We can constrain the location of the Faraday screen by investigating the frequency dependence of RM through a simple model (Jorstad et al. 2007). The RM depends on the electron density  $n_e$ , the parallel magnetic field strength to the line of sight  $B_{\parallel}$ , and the path length as  $\text{RM} \propto \int n_e B_{\parallel} dl$ . This simple jet model leads to a RM dependence on the observing frequency as above, assuming that, for optically thick VLBI cores, the distance  $r$  of the emission region to the central engine depends on the observing frequency  $\nu$  as  $r \propto \nu^{-1}$ , the

electron density  $n_e$  and the magnetic field parallel to the line of sight  $B_{\parallel}$  in the region evolve as  $n_e \propto r^{-n}$  and  $B_{\parallel} \propto r^{-1}$  along the jet, and the path length  $l$  increases as a function of  $r$  as  $l \propto r$ . For spherical or conical geometries of the jet, the appropriate value of the index  $a = 2$ . This model suggests that a Faraday screen affecting the multi-frequency polarization emission from a compact radio source is located in or near the jet when the frequency dependence  $a$  of RM is close to 2, as discussed in Jorstad et al. (2007). With the multi-frequency polarization observations, we found that the RM frequency dependence is in the range of  $a = 0.7 - 3.4$  with a mean of 2.2, as shown in Figure 5. This seems similar to previous measurements of  $a = 1.9 - 3.6$  for several AGN as presented in Lee et al. (2015), although there are some cases with  $a = 0.7 - 1.9$ . This implies that the Faraday rotation of the radio polarization at 22–86 GHz occurs in or near the jet of 3C 279 whose geometry may be spherical or conical.

## 5. SUMMARY

The multi-frequency polarization monitoring observations of 3C 279 enable us to find the following:

1. The 2013 December  $\gamma$ -ray flare of 3C 279 originated in an emission region optically thick at radio frequencies of 22–86 GHz, or may have been generated by different populations of electrons at locations different from those emitting the radio emission.
2. The radio and optical polarization emissions originated from different region responsible for the  $\gamma$ -ray emission region are maintained by the dominant magnetic field perpendicular to the direction of the radio jet at milliarcsecond scales.
3. The polarization emission of 3C 279 at 22–86 GHz bands experience Faraday rotation by a Faraday screen containing a uniform magnetic field that persisted over  $\sim 400$  days after the  $\gamma$ -ray flare, or was not affected by the  $\gamma$ -ray events. To the extent that a simple jet model is applicable to the radio emission from 3C 279, we suggest that the Faraday rotation of the radio polarization at 22–86 GHz is generated in or near the jet of 3C 279 whose geometry may be spherical or conical.

## ACKNOWLEDGMENTS

We are grateful to Sascha Trippe for important comments and suggestions which have enormously improved the manuscript. We thank Jan Wagner for reading and improving the manuscript. The KVN is a facility operated by the Korea Astronomy and Space Science Institute. The KVN operations are supported by KREONET (Korea Research Environment Open Network) which is managed and operated by KISTI (Korea Institute of Science and Technology Information).



## REFERENCES

- Abdo, A. A., Ackermann, M., Ajello, M., et al. 2010, A change in the optical polarization associated with a  $\gamma$ -ray flare in the blazar 3C279, *Nature*, 463, 919
- Aleksić, J., Ansoldi, S., Antonelli, L. A., et al. 2011, MAGIC observations and multi-frequency properties of the flat spectrum radio quasar 3C 279 in 2011, *A&A*, 567, 41
- Aumont, J., Conversi, L., Thum, C., et al. 2010, Measurement of the Crab Nebula Polarization at 90 GHz as a Calibrator for CMB Experiments, *A&A*, 514, A70
- Boettcher, M., Harris, D. E., & Krawczynski, H. 2012, *Relativistic Jets from Active Galactic Nuclei* (Berlin: Wiley)
- Burn, B. J. 1966, On the depolarization of discrete radio sources by Faraday dispersion, *MNRAS*, 133, 67
- Chatterjee, R., Jorstad, S. G., Marscher, A. P., et al. 2008, Correlated Multi-Wave Band Variability in the Blazar 3C 279 from 1996 to 2007, *ApJ*, 689, 79
- D’Ammando, F., Raiteri, C. M., Villata, M., et al. 2011, AGILE detection of extreme  $\gamma$ -ray activity from the blazar PKS 1510-089 during March 2009, *A&A*, 529, 145
- Farnes, J. S., Gaensler, B. M., & Carretti, E. 2014, A Broadband Polarization Catalog of Extragalactic Radio Sources, *ApJS*, 212, 15
- Flett, A. M. & Henderson, C. 1979, Observations of the polarized emission of Taurus A, Cas A and Cygnus A at 9-mm wavelength, *MNRAS*, 189, 867
- Hada K., Kino M., Nagai H., et al. 2012, VLBI Observations of the Jet in M 87 during the Very High Energy  $\gamma$ -ray Flare in 2010 April, *Apj*, 760, 52H
- Hayashida M., Nalewajko K., Madejski G. M., et al. 2015, Rapid Variability of Blazar 3C 279 during Flaring States in 2013-2014 with Joint *Fermi*-LAT, *NuSTAR*, *SWIFT*, and Ground-based Multi-wavelength Observations *Apj*, 807, 79H
- Jorstad, S. G., Marscher, A. P., Stevens, J. A., et al. 2007, Multiwaveband Polarimetric Observations of 15 Active Galactic Nuclei at High Frequencies: Correlated Polarization Behavior, *AJ*, 134, 799
- Krawczynski, H., Boettcher, M., & Reimer, A. 2012, Unresolved Emission from the Core: Observations and Models, *Relativistic Jets from Active Galactic Nuclei* (Berlin: Wiley), 218
- Krolik, J. H. 1999, *Active galactic nuclei : from the central black hole to the galactic environment* (Princeton: Princeton University Press)
- Lee, S.-S., Byun, D.-Y., Oh, C. S., et al. 2011, Single-Dish Performance of KVN 21-m Radio Telescopes: Simultaneous Observations at 22 and 43 GHz, *PASP*, 123, 1398
- Lee, S.-S., Han, M., Kang, S., et al. 2013, Proceedings of The Innermost Regions of Relativistic Jets and Their Magnetic Fields (EPJ Web of Conferences), ed. J. L. Gomez, 61
- Lee, S.-S., Petrov, L., Byun, D.-Y., et al. 2014, Early Science with the Korean VLBI Network: Evaluation of System Performance, *AJ*, 147, 77
- Lee, S.-S., Kang, S., Byun, D.-Y., et al. 2015, First Detection of 350 Micron Polarization from a Radio-loud AGN, *ApJ*, 808, 26L
- Larionov, V. M., Jorstad, S. G., Marscher, A. P., et al. 2008, Results of WEBT, VLBA and RXTE monitoring of 3C 279 during 2006-2007, *A&A*, 492, 389
- Mangum, J. G., 2000, *User’s Manual for the NRAO 12 Meter Millimeter-Wave Telescope*, NRAO, 129
- Marscher, A. P., Jorstad, S. G., D’Arcangelo, F. D., et al. 2008, The inner jet of an active galactic nucleus as revealed by a radio-to- $\gamma$ -ray outburst, *Nature*, 452, 966
- Mascher, A., Jorstad, S., Larionov, V., et al. 2010, Probing the Inner Jet of the Quasar PKS 1510-089 with Multi-waveband Monitoring During Strong Gamma-ray Activity, *ApJ*, 710, 126
- Orienti, M., Venturi, T., Dallacasa, D., et al. 2011, Multi-epoch parsec-scale observations of the blazar PKS 1510089, *MNRAS*, 417, 359
- Perley, R. A.; Butler, B. J. 2013, Integrated Polarization Properties of 3C48, 3C138, 3C147, and 3C286, *ApJS*, 206, 16
- Sasada, M., Uemura, M., Arai, A., et al. 2010, Multi-band Photopolarimetric Monitoring of an Outburst of the Blazar 3C 454.3 in 2007, *PASJ*, 62, 645
- Sault R. J., Hamaker J. P., and Bregman J. D. 1996, Understanding radio polarimetry. II. Instrumental calibration of an interferometer array, *A&AS*, 117, 149
- Tribble, P. C. 1991, Depolarization of extended radio sources by a foreground Faraday screen, *MNRAS*, 250, 726
- Wehrle, A. E., Marscher, A. P., Jorstad, S. G., et al. 2012, Multiwavelength Variations of 3C 454.3 during the 2010 November to 2011 January Outburst, *ApJ*, 758, 72